Chemical Science

ROYAL SOCIETY OF CHEMISTRY

EDGE ARTICLE

View Article Online
View Journal

Cite this: DOI: 10.1039/d5sc07740k

All publication charges for this article have been paid for by the Royal Society of Chemistry

Sulfonyl-tuned amino DASAs for targeted photophysical and photoswitching control

Alexander Karr,† Hye Joon Lee,† A. Talim G. K, Chloe A. Ramsperger, Cesar A. Reyes, Kelly Biv and Elias Picazo *

Donor–acceptor Stenhouse adducts (DASAs) are molecular photoswitches with applications spanning materials to molecular machines. Although structural modularity has enabled seminal DASA studies, sulfonyl substituents in amino DASAs remain unexplored. Evaluation of sulfonyl substituents reveals a distinct photoswitching pathway between acyclic isomers about the C_3–C_4 bond, as evidenced by UV-vis spectroscopy and low-temperature NMR spectroscopy. This discovery was achieved by significantly improving DASA structural stability under irradiation, which in turn enables the creation of a compound that sets the record for amino DASA isomer distribution at the photostationary state. Thermal reversion is rapid with little to no fatigue in dichloromethane and solvent versatility is demonstrated with photoswitching and full recovery in toluene, albeit with slower thermal recovery rates. Sulfonyl substituents are also found to modulate molar absorption coefficients and structural charge distribution in a manner that broadly follows Hammett substituent constants with modest correlations, thereby providing qualitative guidance for molecular design. These findings enable the greater DASA photoswitch class to selectively access multiple isomers through structural design, offering opportunities for further developments in responsive materials, soft robotics, and selective reactivity.

Received 7th October 2025
Accepted 11th December 2025

DOI: 10.1039/d5sc07740k

rsc.li/chemical-science

Introduction

Precise control of material properties using an external stimulus is of significant interest for responsive material development. Molecular photoswitches are compounds that can undergo reversible structural changes using light, a benign and maneuverable stimulus, providing spatiotemporal control and supporting smart materials, phototherapies, and responsive molecular systems.[1–7] Upon absorption of light, photoswitches typically undergo either an *E*/*Z* isomerization or a pericyclic rearrangement, interconverting between two distinct states. Examples of *E*/*Z* isomerization switches include azobenzenes, stilbenes, and (hemi)indigo switches,[8–10] while examples of pericyclic rearrangement switches include diarylethenes and spiropyrans, among others (Fig. 1A).[11,12]

The donor–acceptor Stenhouse adduct (DASA) class was discovered in 2014 [13] and has since gained great interest for its synthetic modularity, multistep switching mechanism, and use in photoresponsive polymers and logic-gated devices, among other applications.[14–24] Unlike photoswitches requiring UV light to undergo single-step transformations,[12,25–28] DASAs use visible light to toggle between **A**, **B**, and **C** states, where **A** represents the thermodynamically favored acyclic form, **B** is a series of metastable acyclic alkene isomers, and **C** is a series of metastable cyclic forms (Fig. 1B).[29–36] The triene photoswitch unit in DASAs enables both actinic *E*/*Z* isomerizations from **A** to **B** and a thermal pericyclic rearrangement from *EZE* **B** to **C**. Although metastable acyclic isomeric **B** forms have been characterized,[37] precise DASA switching between the **A** form and a single **B** isomer without **C** formation remains elusive despite vastly different properties between **B** and **C** isomers that are of interest for (bio)electronic and conductive responsive materials.[38] The continued advancement of DASA structural modularity has repeatedly unlocked insights into swtiching mechanisms, functional behaviors, applications, and tunable properties,[13,39–47] raising the prospect that further structural innovation may ultimately deliver the selective **A** to single-**B** photoswitching.

DASAs produce equilibria with low **B**-series exclusivity as a result of an electron rich C_5 from C_2-hydroxyl electron donation through resonance,[29–36] which distinguishes them from traditional merocyanine dyes.[48] In the development of a multistage system, an equilibrium of **A**, **B**, and **C** isomers was established using strategically tuned donor and acceptor units bearing sterically demanding groups to increase the kinetic barriers of isomerization.[49] In a separate study, removal of the backbone heteroatom was shown to circumvent 4π-electrocyclization while unselectively forming multiple **B**-series isomers,[32] highlighting the critical heteroatomic electronic

Department of Chemistry, Loker Hydrocarbon Research Institute, University of Southern California, 837 Bloom Walk, Los Angeles, California 90089-1661, USA. E-mail: epicazo@usc.edu

† These authors contributed equally to this work.

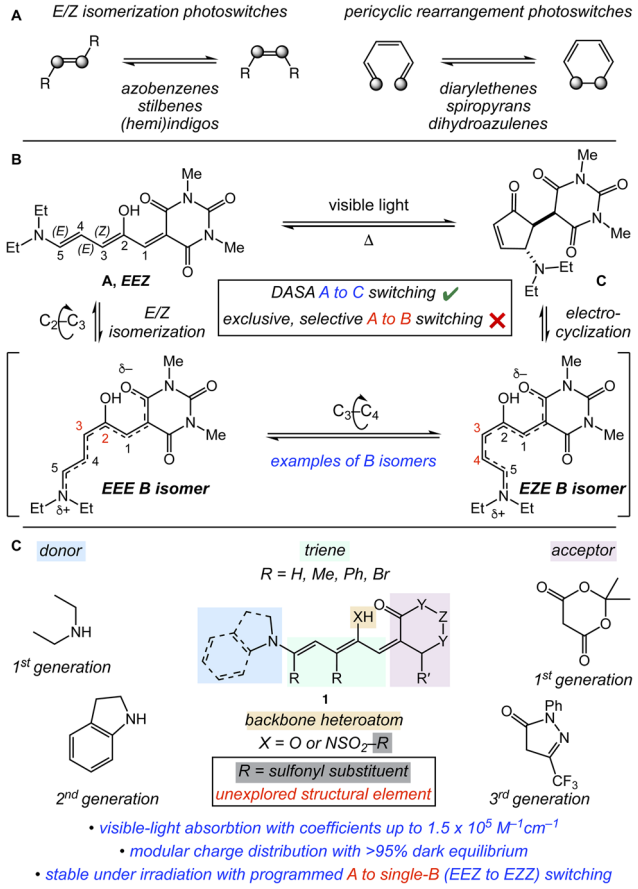

Fig. 1 (A) *E*/*Z* isomerization and pericyclic rearrangement photoswitch types. (B) Donor–acceptor Stenhouse adducts (DASAs) isomerizing between **A** and **C** isomers through **B** isomers. (C) DASA structural modularity, including the unexplored sulfonyl substituents in amino DASAs (this work), enabling exclusive, selective **A** to single-**B** switching and photophysical property tuning.

effect on interrupting the full **A** to **C** DASA switching sequence. We recently developed a pyrrole rearrangement that introduces C_2 heteroatomic variation on the DASA structure.[50,51] Despite creating an amino DASA of each generation using a 4-bromobenzenesulfonyl group on the C_2 nitrogen atom, photoisomerization was not discernible by NMR due to inefficient photoswitching. The additional bonding orbital on the C_2 nitrogen atom in amino DASAs is an unexplored structural domain that is of high interest for its potential to achieve selective **A** to **B** DASA photoswitching while simultaneously advancing amino DASA switching function and photophysical tunability by strategically altering steric and electronic profiles.

Herein, we report the exploration of sulfonyl substitution effects on amino donor–acceptor Stenhouse adducts (DASAs) and the discovery of a new photoswitching paradigm within this widely studied negative photochrome family. By introducing sulfonyl groups on the C_2 nitrogen atom, we suppress the conventional multi-step pathway involving cyclization or competing acyclic isomers and instead achieve clean isomerization about the C_3–C_4 bond (*EEZ* open form **A** to *EZZ* open form **B**) and retain a fully conjugated, acyclic structure in both states. This selective conjugated-to-conjugated switching is accompanied by exceptional photostability, enabling the creation of an amino DASA with the highest reported population of the photogenerated isomer for the amino DASA subclass. A rapid, nearly quantitative thermal reversion after extended periods of irradiation in dichloromethane is coupled with solvent versatility that extends to non-polar media such as toluene, albeit with slower thermal recovery rates. Low-temperature NMR and UV-vis spectroscopy confirm the exclusive formation of the *EZZ* **B** isomer from the *EEZ* **A** isomer upon irradiation, while systematic variation of the sulfonyl substituent reveals qualitative electronic trends in molar absorptivity and charge distribution. These findings establish a rational, modular strategy for accessing selective, open-form DASA photoswitches and expand their potential in responsive materials, soft robotics, and light-gated selective reactivity.

Results and discussion

Sulfonyl substituent library and their photophysical properties

The streamlined three-step synthesis of sulfonyl amino DASAs, starting from commercially available pyrrole-2-carboxaldehyde **2**, is shown in Fig. 2A. Together, a sulfonylation reaction with a respective sulfonyl chloride produces pyrrole **3**, a subsequent Knoevenagel condensation with an acceptor provides activated pyrrole **4**, and a donor-mediated pyrrole rearrangement reliably yields the desired sulfonyl amino DASA product **5**. DASAs are typically isolated by recrystallization and trituration because of compound crystallinity[41,52] and instability on silica gel. Inspired by (1) an increased rate of heterocyclic ring opening for DASA synthesis when employing hexafluoroisopropanol (HFIP), (2) HFIP-mediated stabilization of the DASA **A** form through hydrogen bonding,[20,53] and (3) remaining impurities in several of the reported amino DASAs following precipitation efforts, we discovered that adding 0.5–5% HFIP by volume to a suitable mobile phase, typically 0.5–2% methanol in dichloromethane by volume, enables amino DASA purification through column chromatography. Although chromatographic isolated yields are lower (15–55% yield), recovery is sufficient to characterize compounds that remained impure after precipitation efforts. Amino DASAs were not chromatographically stable without the addition of HFIP.

To draw trends between sulfonyl substitents and DASA photophysical properties, and to investigate their impact on photoswitching, we synthesized a library using *N*,*N*-dimethyl barbituric acid as the acceptor and unsubstituted indoline as the donor. These amino DASAs are therefore reminiscent to second-generation hydroxy DASAs, which are comprised of a weakly donating arylamine donor and a relatively weakly withdrawing acceptor.[42,43] The scope and overview of compound photophysical properties are shown in Fig. 2B. Benzenesulfonyl amino DASA **6** serves as the parent compound, synthesized in 61% yield, with extended sulfonyl conjugation explored through 1-naphthyl DASA **7**. Sulfonyl amino DASAs containing electron donating groups on the sulfonyl group, such as 4-methoxy **8** and 4-methylthio **9**, are isolated in 15 and 29% yields, respectively. Halogenated sulfonyl groups like 4-fluoro- **10**, 4-chloro- **11**, and

4-iodobenzene **13** yield product in 70, 29, and 74%, respectively. Compounds containing groups with stronger withdrawing capacity, including 4-azido- **14**, 4-nitro- **15**, 2-nitro- **16**, 4-trifluoromethyl- **17**, and 4-cyanobenzene **18**, are prepared in 47–76% yield. 4- and 2-nitrobenzenesulfonyl DASAs **15** and **16** allowed us to evaluate an electronic effect when comparing to benzenesulfonyl amino DASA **6** while simultaneously validating an observed steric effect on stability during irradiation (*vide infra*). Halide-containing sulfonyl amino DASAs **10–13** and azide-containing DASA **14** offer useful reactive cross-coupling or click reaction handles at previously unobtainable molecular regions,[54] highlighting the potential utility of the additional bonding orbital on nitrogen beyond pyrrole activation and DASA property adjustments. Although DASAs have been functionalized at the donor and acceptor compartments,[20] and have themselves been embedded into polymer backbones,[55] functionalizing at the sulfonyl group provides a fourth distinct spatial arrangement with photophysical advantages like unaltered λ_{max} values despite undergoing electronic changes at sulfonyl group (*vide infra*). Sulfonamides substituted with multiple halides, such as 2,4,5-trichloro- **19** (68% yield) and pentafluorobenzene **20** (99% yield), enable comparisons with monosubstituted analogs. Heterocycles including 3-pyridine- and 2-thiophene-containing products **21** and **22**, synthesized in 57 and 72% yield, respectively, further diversify the library. Finally, we synthesized sulfonyl amino DASAs featuring mesityl **23**, 4-*t*-butyl mesityl **24**, and methyl **25** sulfonyl groups to assess steric effects.

The absorption bands of sulfonyl amino DASAs have λ_{max} values ranging from 577–582 nm in dichloromethane. This is demonstrated in Fig. 3A through the narrow range of absorption λ_{max} values displayed by amino DASAs **6**, **8**, **18**, **21**, and **25**, containing structurally diverse sulfonyl groups. Sulfonyl amino DASAs exhibit a slight hypsochromic shift in λ_{max} relative to hydroxy DASA analogs (615 nm),[50] attributed to the strong electron-withdrawing nature of the sulfonamide group, despite nitrogen being a less electronegative atom than oxygen.[50,56] The narrow range of absorption λ_{max} values is consistent with sulfonyl group substituents primarily exerting inductive effects with negligible resonance contributions to the triene system.

Time-dependent density functional theory (TD-DFT) calculations, which model responses to time-dependent perturbations like light,[57] were performed on benzenesulfonyl, 4-methoxybenzenesulfonyl, and 4-cyanobenzenesulfonyl DASAs **6**, **8**, and **18** to visualize the $S_0 \rightarrow S_1$ transition. These calculations reveal that sulfonyl substituents have little impact on the electron distribution involved in the S_1 excited state. As shown in Fig. 3B, electron density in both the hole, the orbital from which the electron is excited, and the electron, the orbital occupied upon excitation, remains localized in the same regions across compounds. This supports the minimal influence of sulfonyl groups on λ_{max} values. Additionally, ground-state DFT calculations on DASAs **6**, **8**, and **18** confirm that sulfonyl substituents do not significantly alter the HOMO or LUMO (see SI Fig. S269). Notably, molar absorption coefficients in dichloromethane span a wide range between 18 000 and 140 000 M^{-1} cm^{-1}, with 2-nitrobenzene and thiophene-containing sulfonyl amino DASAs **16** and **22** showing significant variation. The low molar absorption coefficient of 2-nitrobenzene sulfonyl amino DASA **16** is thought to arise from an ortho-steric effect that also impacts amino DASAs **19** and **23**. In contrast, sulfonyl amino DASA **22** contains a polarizable sulfur atom in the thiophene unit, which is known to increase molar absorption coefficients.[58]

Solvatochromic slope values, quantifying charge distribution in the conjugated **A** form, were derived from normalized Dimroth–Reichardt E_T^N parameters[59,60] and range between −6 and −20 nm. A steeper slope from increased solvatochromism is consistent with increased push–pull character. The slopes reflect a predominantly hybrid character with minimal charge confinement, consistent with second-generation hydroxy DASAs, and showcase the ability to fine-tune within the hybrid zone through sulfonyl group modifications. This is significant since current modifications in donor or acceptor units typically lead to large changes in charge separation. A general trend is observed (Fig. 3C) wherein sulfonyl amino DASAs containing electron neutral or donating groups on the sulfonyl, such as **6–9**, exhibit lower slopes between −6 and −9 nm, consistent with lower charge separation. Conversely, sulfonyl amino DASAs containing strong electron withdrawing groups on the sulfonyl generally display larger solvatochromic slopes, such as −19 nm for 4-cyanobenzenesulfonyl amino DASA **18**, indicating enhanced zwitterionic character in the conjugated **A** form. The electronic effects of sulfonyl substituents on solvatochromic slope and molar absorption coefficient of amino DASAs were also explored for future predictability by plotting Hammett substituent constants (σ)[61] against these properties. Although strong correlations ($R^2 > 0.9$) are not observed, the data reveal a qualitative trend (Fig. 3D). A larger, more positive Hammett constant is associated with both a higher molar absorption coefficient and a larger absolute solvatochromic slope value. Therefore, in the absence of *ortho*-steric effects, increasing electron withdrawing strength of the sulfonyl substituent only modestly leads to increased light absorptivity and greater **A**-form zwitterionic character.

Sulfonyl effects on stability during irradiation and combinatorial effects on isomer distribution at the photostationary state

To elucidate sulfonyl effects on photoswitching efficiency, we evaluated the full sulfonyl amino DASA library (see SI Fig. 96–120) and highlight 4-bromobenzene **12**,[50] 4-methylthiobenzene **9**, 4-cyanobenzene **18**, 3-pyridyl **21**, and mesityl **23** as exemplary structures in Fig. 4A. These structures demonstrate the effects of electron donating, electron withdrawing, and *ortho* sterics in comparison to known compound **12**. Using a 590 nm LED, we measured the isomer distribution at the photostationary state (PSS) by the decay in λ_{max}, which represents the consumption of isomer **A**. Though sulfonyl group electronics did not significantly impact distribution values, achieving approximately 26% in toluene, they did have an observable effect on reversion and compound stability under irradiation (Fig. 4A). A rapid and efficient reversion was observed for 4-cyanobenzenesulfonyl

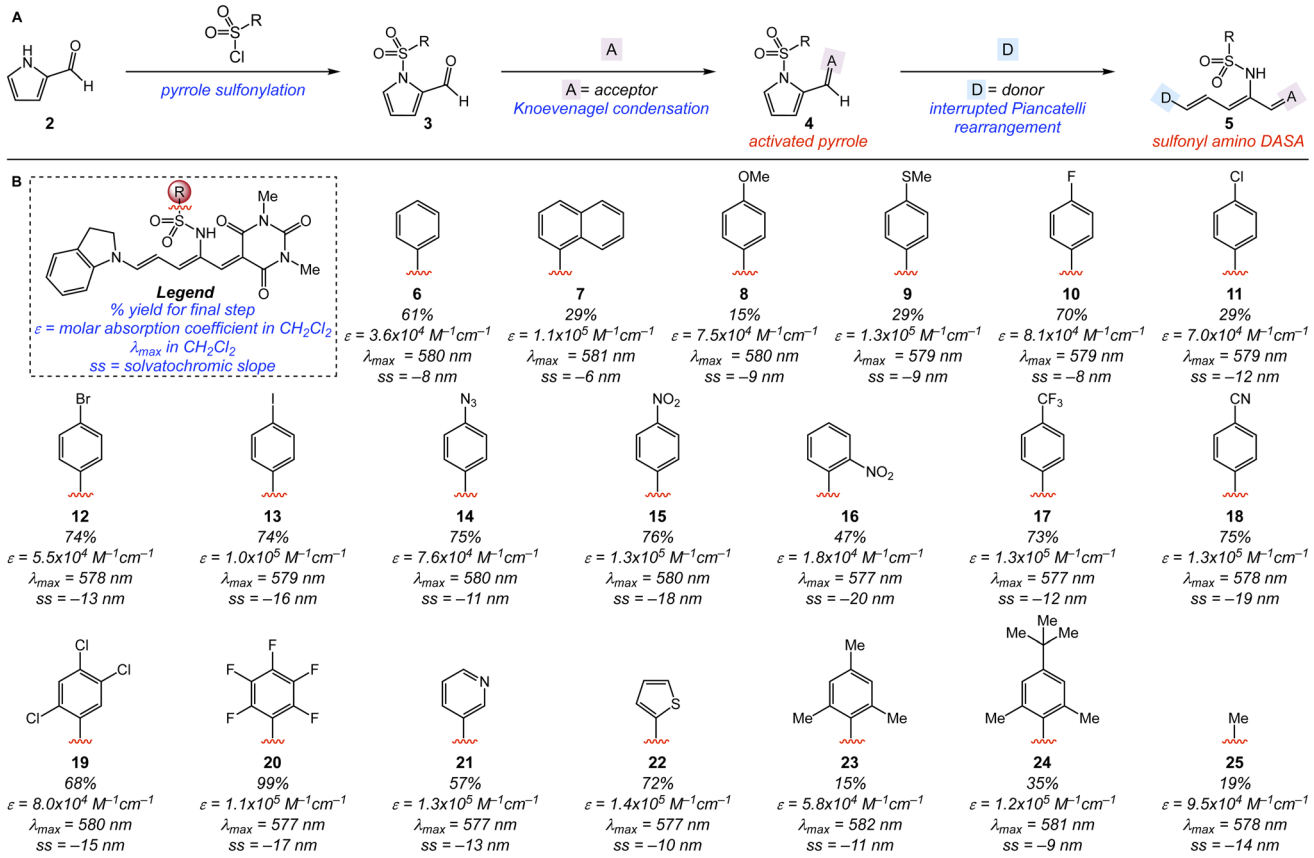

Fig. 2 (A) Streamlined three-step synthesis of sulfonyl amino DASAs. (B) Sulfonyl amino DASA scope and key photophysical properties, including molar absorption coefficient in dichloromethane, λ_{max} in dichloromethane, solvatochromic slope, and isolation yield of the final step.

amino DASA **18**, which fully recovered within 45 seconds in toluene. Steric hindrance, particularly from *ortho*-substituted groups, reduces compound stability under irradiation, limiting reversible switching compared to less hindered analogs. This is demonstrated by *D*%, the additional decay of λ_{max} after establishing the PSS. For example, mesityl-containing DASA **23** reduced an additional 59% under irradiation in comparison to a loss of only 3% for DASA **18** under identical conditions. Heterocyclic DASAs **21** and **22** performed well with 3-pyridyl DASA **21** achieving a distribution and stability profile comparable to 4-cyanobenzene **18**. We hypothesize that 3-pyridyl DASA **21** performs well due to the electron withdrawing nature of the pyridine ring while 2-thiophene DASA **22** performs well due to the smaller steric profile. Toluene was selected for photostationary state studies due to consistently increased distributions in comparison to dichloromethane (see SI Fig. 121–122). All compounds exhibit >99% of the thermodynamically favored **A** form (Fig. 1B) at dark equilibrium by NMR in $CDCl_3$, ensuring high levels of reversion to the **A** form in the absence of light. This high dark equilibrium is attributed to a strong H-bond interaction between the sulfonamide and acceptor carbonyl that stabilizes the **A** isomer.[29–36,50] Together, these trends highlight the sulfonamide's role in tuning switching performance and stability.

The stable switching of cyano-substituted DASA **18** warranted subsequent combinatorial studies with varying donors and acceptors. For donor evaluation, maintaining the *N*,*N*-dimethyl barbituric acid acceptor (Fig. 4B), we assessed 4-cyanobenzenesulfonamide DASAs composed of unsubstituted indoline **18**, 5-methoxyindoline **26**, 5-fluoroindoline **27**, and isoindoline **28**. Isomer distribution values, per consumption of λ_{max}, between 2 and 26% were observed at PSS under 590 nm LED irradiation in toluene. Electron withdrawing substituents on the donor result in larger decreases in λ_{max} intensity under irradiation than donating groups, with isoindoline producing the lowest conversion. We reason that greater partial negative charge in the acceptor carbonyl, further verified by solvatochromic slopes, renders the acceptor carbonyl a stronger hydrogen-bond acceptor. This in turn strengthens the H-bond interaction and reduces switching efficiency in amino DASAs. Together, we conclude that an amino photoswitch with a weaker donor and/or acceptor, resulting in decreased charge separation in the **A** form, per solvatochromic analysis, will result in increased λ_{max} consumption under irradiation. Attempts at weakening the interaction from the donor compartment were limited by failed pyrrole rearrangements when using highly electron withdrawn nucleophiles, such as 5-nitroindoline.

Using unsubstituted indoline as the donor, an acceptor evaluation revealed that highly withdrawing acceptors, such as trifluoromethyl pyrazolone in sulfonyl amino DASA **29**, hamper λ_{max} consumption under irradiation (Fig. 4C). We then sought

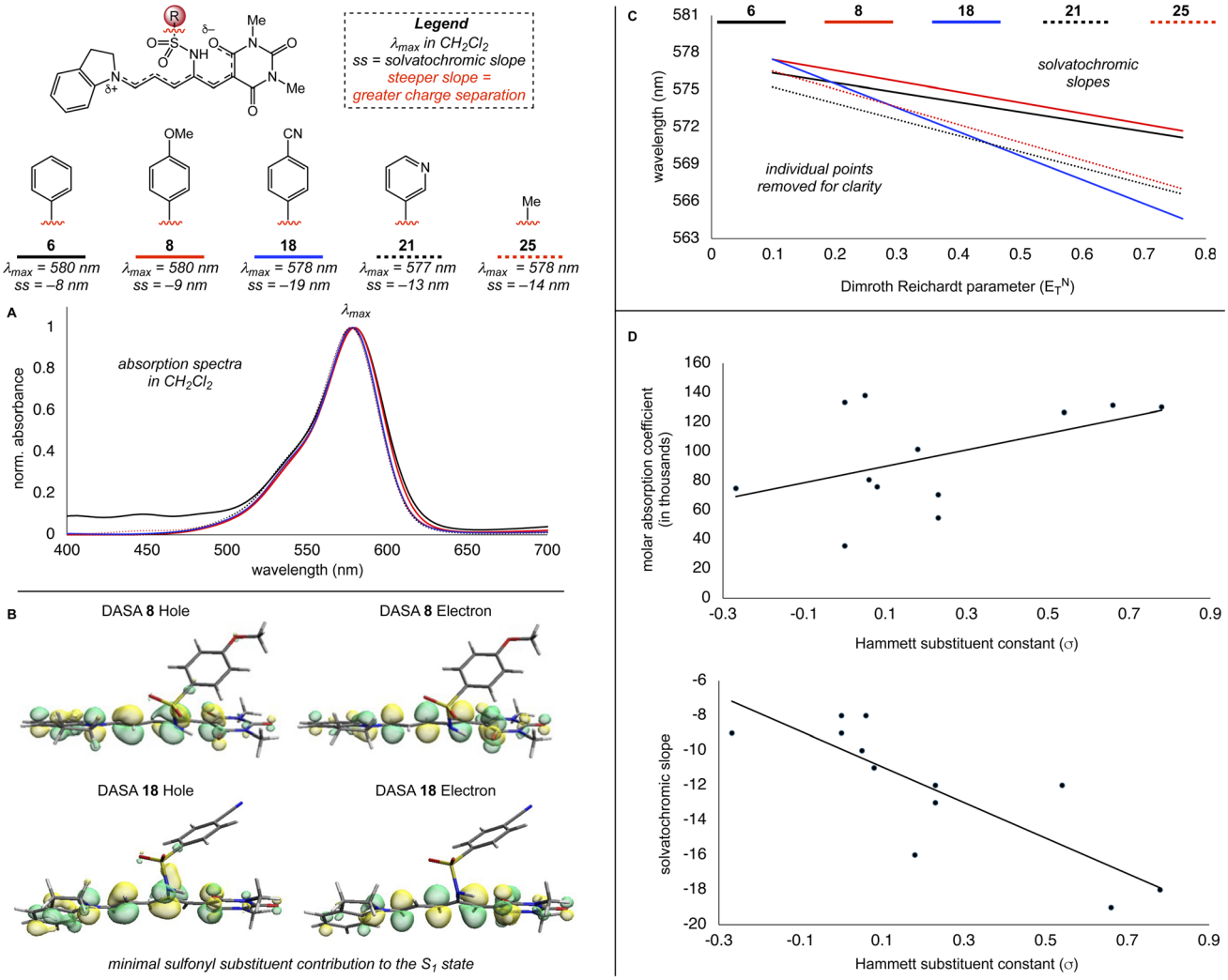

Fig. 3 (A) Sulfonyl substituent impact on absorption λ_{max}. (B) Natural transition orbitals (NTOs, hole and electron) in the S_1 state for DASAs **8** and **18** calculated using TD-DFT at the B3LYP/6–31G** level in the gas phase (isovalue = 0.1). (C) Sulfonyl substituent impact on molecular charge distribution. (D) General trends between sulfonyl substituent electronics and molar absorption coefficient or solvatochromic slope (charge distribution of **A** form).

to weaken the H-bond accepting capacity of the carbonyl units in the acceptor through extended conjugation and by removal of donating heteroatoms. As such, we synthesized 1,3-indandione-containing sulfonyl amino DASA **30**, which provides a λ_{max} decay of 49% in toluene under irradiation, consistent with our hydrogen-bonding hypothesis. Though faster in dichloromethane (see SI Fig. 120), full reversion is observed for amino DASA **30** in both toluene (31 minutes) and dichloromethane (45 seconds). Faster reversion in dichloromethane compared to toluene is consistent with prior studies demonstrating that this effect is attributable to the use of an arylamine donor.[43,44,62] Amino DASA **30** with the 1,3-indandione acceptor exhibits an unusual solvatochromic slope of 3 nm and increased stability under irradiation, decreasing <1% in λ_{max} intensity after 10 minutes of irradiation, while the hydroxy DASA equivalent undergoes irreversible consumption upon irradiation.[44] These variations demonstrate a synergistic effect between the donor, acceptor, and sulfonyl groups in tuning DASA properties through modifications of intramolecular H-bonding interactions, molecular charge distribution, and the HOMO–LUMO gap. As a result of increased compound stability under irradiation with 4-cyanobenzenesulfonamide, optimal λ_{max} decay with a 1,3-indandione acceptor, and increased reversion rate in dichloromethane, we conducted a cycling study of amino DASA **30** in dichloromethane (Fig. 4D). As expected, little to no fatigue was observed over nine cycles with 45 seconds of irradiation followed by 45 seconds of recovery, further highlighting the increased stability and function of sulfonyl amino DASAs. Overall, sulfonyl evaluation enabled the creation of DASA **30** which sets the record for amino DASA distribution at the PSS, photoswitches and fully recovers rapidly in dichloromethane, showcases solvent versatility with photoswitching and full recovery in toluene, and shows little to no fatigue in both solvents.

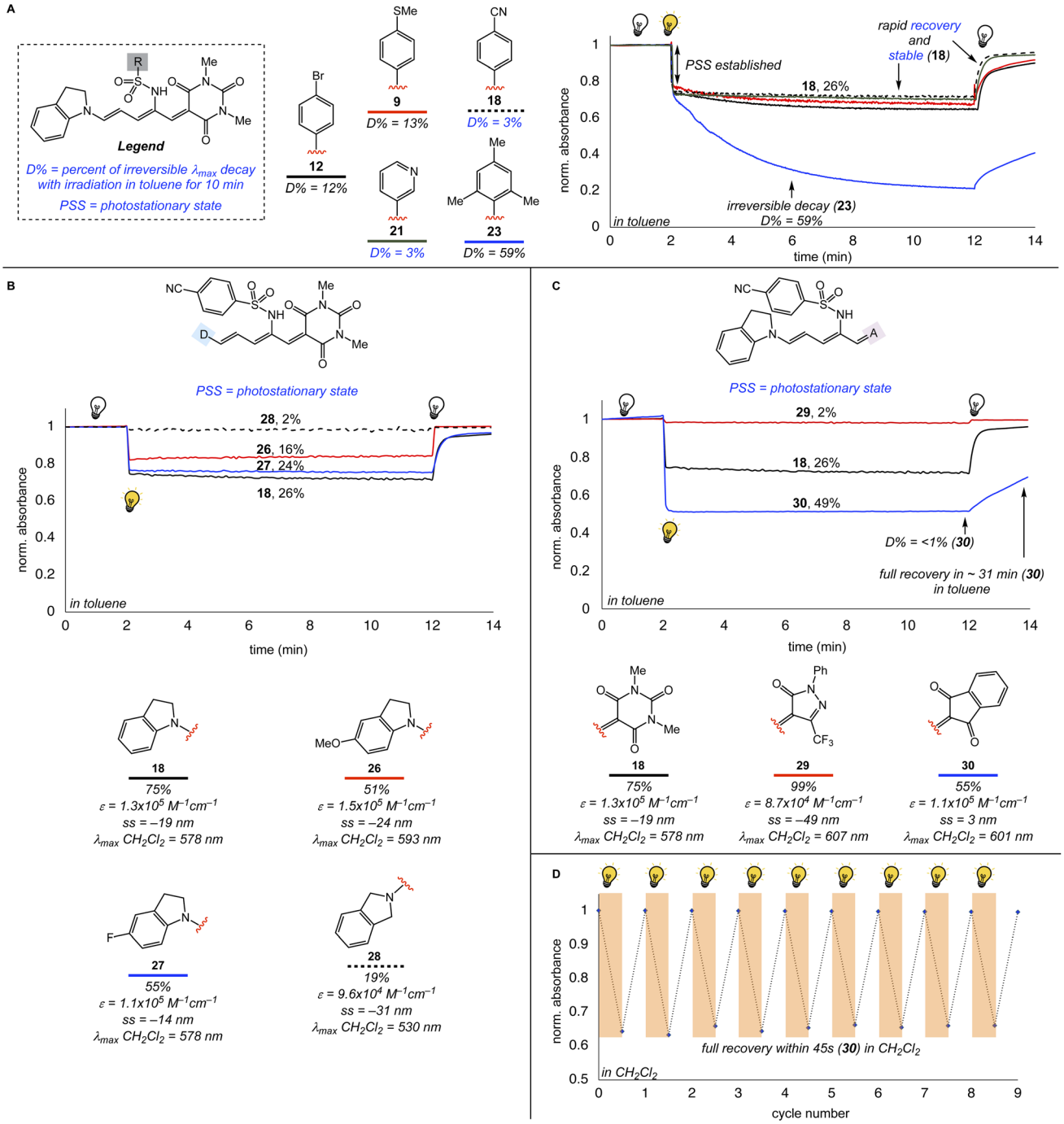

Fig. 4 (A) Sulfonyl substituent effects on DASA stability under irradiation. (B) Donor evaluation using 4-cyanobenzenesulfonyl and *N*,*N*-dimethyl barbituric acid groups. (C) Acceptor evaluation using 4-cyanobenzenesulfonyl and unsubstituted indoline groups. (D) Cycling study of amino DASA **30** in CH_2Cl_2 with 45 seconds of irradiation and 45 seconds recovery over 9 cycles. Highlighted regions indicate irradiation periods using a 590 nm LED. Full recovery of DASA **30** in toluene and additional studies in both solvents can be found in the SI.

Switching characterization

Interested in the structural changes responsible for reversible depletion of λ_{max} (Fig. 5A), we conducted a full spectrum UV-vis analysis of amino DASAs **18** and **30** with and without irradiation in dichloromethane. As expected from the λ_{max} distribution studies, pre-irradiation and post-irradiation spectra of amino DASA **30** matched, indicating reversibility (see SI Fig. 123). Furthermore, a full spectrum scan during irradiation shows depletion of λ_{max} intensity with concomitant broadening toward longer wavelengths under irradiation (Fig. 5B). This was indicative of the formation of **B**-series isomer(s), which have been previously characterized to have red-shifted λ_{max} values.[30,32,49] To get definitive evidence of the formation of **B**-series isomers, we conducted *in situ* irradiative, low-temperature NMR studies at 208 K in CD_2Cl_2 using 590 nm LED irradiation (Fig. 5C).

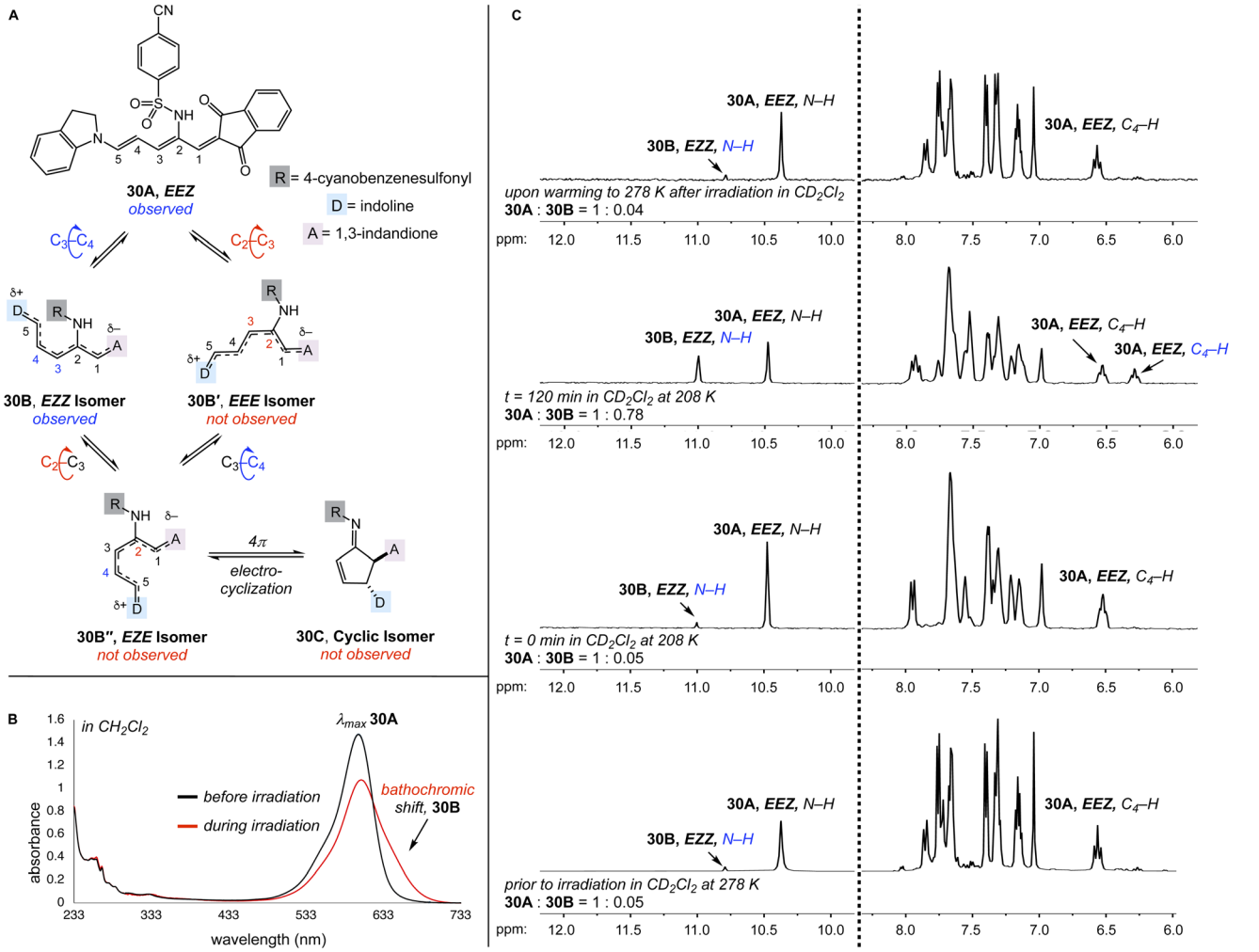

Fig. 5 (A) Potential isomeric pathways and structures in sulfonyl amino DASA photoswitching. (B) Full spectrum UV-vis scan indicating distinct chromophore formation upon consumption of **30A** under irradiation in dichloromethane. (C) Low-temperature NMR study of sulfonyl amino DASA **30** at 208 K showcasing selective **A** to **B** (*EEZ* to *EZZ*) photoswitching in deuterated dichloromethane. Deuterated dichloromethane was used due to solubility constraints in deuterated toluene.

Deuterated toluene was not a suitable solvent for this study due to insufficient compound solubility. Consistent with the formation of the *EZZ* isomer **30B**, a new downfield N–H singlet grew from a 1 : 0.05 to a 1 : 0.78 ratio at 11.0 ppm without the formation of an upfield signal between 10.3–8.0 ppm corresponding to the *EEE* isomer, **30B′**. Furthermore, an apparent C_4–H triplet consistent with *EZZ* isomer **30B** formation appears near 6.29 ppm. In addition to not observing signals for *EEE* isomer **30B′**, the *EZE* (**30B″**) and cyclic (**30C**) isomers are not observed. The 1 : 0.78 ratio represents a 44% conversion, which is close to the 37% distribution established under UV-vis conditions in dichloromethane (see SI Fig. 120). The slight deviation between UV-vis λ_{max} depletion studies and NMR studies may be a result of concentration effects or experimental setup. The ^{1}H NMR spectra at 278 K preceding and following *in situ* irradiation studies confirm thermal reversion to the **A** form. Critically, this analysis was reproduced with lower conversion but consistent **A** to **B** isomerization results for sulfonyl amino DASA **18** containing *N*,*N*-dimethyl barbituric acid as the acceptor (see SI Fig. 125, 126, and 134), underscoring that the **A** to single-**B** switching is a sulfonyl effect as opposed to a 1,3-indandione effect. Amino DASA **18** formed a ratio of 1 : 0.06 under *in situ* irradiative, low-temperature NMR conditions at 208 K in CD_2Cl_2 using 590 nm LED irradiation. None of the remaining compounds were evaluated by NMR due to lower isomerization efficiencies, lower stabilities, or both. Attempts to prepare 1,3-indandione-derived amino DASAs bearing 3-pyridyl or 1-naphthyl sulfonyl groups failed because the respective pyrrole substrates did not undergo the desired rearrangement. Such efforts remain interesting future directions.

Conclusions

In conclusion, this work leverages the unique functionality and electronics of the C_2 nitrogen atom in amino DASAs to achieve a selective **A** to single-**B** photoisomerization. This controlled **A** to single-**B** switching in sulfonyl amino DASAs selectively interrupts the multi-step switching sequence available to DASAs

for the first time. Through a systematic steric and electronic evaluation of the uncharted sulfonyl group, we identified DASAs with high structural stability under irradiation. This high level of irradiative stability enabled the discovery of an amino DASA with a 49 : 51 (**B** : **A**) isomer distribution at the photostationary state with rapid and full thermal recovery in dichloromethane (45 seconds) and with little to no fatigue over 9 cycles. An amino DASA record isomeric distribution under irradiation was achieved by decreasing the strength of the hydrogen-bond interaction with the use of 1,3-indandione as the acceptor unit. Although thermal reversion is slower in toluene (31 minutes), the optimal amino DASA shows great solvent versatility with full reversion in toluene. Together, these advances enabled the characterization, by UV-vis spectroscopy and low-temperature NMR spectroscopy, of the distinct **A** to single-**B** (*EEZ* **A** to *EZZ* **B**) isomer photoswitching about the C_3–C_4 bond without forming the traditional cyclic or other acyclic isomers. Sulfonyl substituents were also found to modulate molar absorption coefficients and structural charge distribution in a manner that broadly follows Hammett substituent constants with modest correlations, thereby providing qualitative guidance for application-specific molecular design. This mode of selective conjugated-to-conjugated switching is of interest for DASA incorporation in smart materials and the *EZZ* **B** isomer presents an opportunity to develop light-initiated, site-selective reactivity by arranging the donor near the sulfonyl fragment upon switching.

Author contributions

A. K. and H. L. contributed to this work equally. A. K., H. L., A. T. G. K., C. A.Ramsperger, C. A. Reyes, and K. B. designed the experiments, optimized the reaction methodology, and analyzed the data. All authors contributed to the preparation of the manuscript and participated in discussions. E. P. directed the investigations.

Conflicts of interest

A provisional patent was previously filed (2024). Patent applicant: University of Southern California; inventors E. P., C. A. Reyes, and H. L.; US Patent Application No.: 63/567 010 for "Photoresponsive Compounds". Specifically, this patent claims the use of our synthetic route for amino DASAs, amino DASAs themselves, and the predictive tool based on carbon NMR for DASA preparation. E. P., C. A. Reyes, and H. L. declare no further competing interests and A. K., A. T. G. K., C. A. Ramsperger, and K. B. declare no competing interests.

Data availability

Full details on the synthesis and characterization of compounds are accessible in the supplementary information (SI). Supplementary information is available. See DOI: https://doi.org/10.1039/d5sc07740k.

Acknowledgements

We acknowledge the University of Southern California, the Loker Hydrocarbon Research Institute, and the USC Norris Comprehensive Cancer Center for support. We are grateful to NIH-NIGMS GM140070 and the Turula family for financial support. A. T. G. K. and C. A. Reyes thank the Loker Hydrocarbon Research Institute for the Harold E. Moulton Fellowship. A. K., A. T. G. K., C. A. Ramsperger, C. A. Reyes, and K. B. thank the University for the Dornsife Fellowship. We thank Dr Shawn Wagner for guidance with complex NMR experimentation. Instrumentation in the USC Chemistry Instrument Facility was acquired with USC Research and Innovation Instrumentation Award Program, the NSF (DBI-0821671, CHE-0840366, CHE-2018740), and NIH (S10 RR25432) support.

Notes and references

1 A. Goulet-Hanssens, F. Eisenreich and S. Hecht, *Adv. Mat.*, 2012, **32**, 1905966.
2 J. Boelke and S. Hecht, *Adv. Opt. Mat.*, 2019, **7**, 1900404.
3 P. Kobauri, F. J. Dekker, W. Szymanski and B. L. Feringa, *Angew. Chem., Int. Ed.*, 2023, **62**, e202300681.
4 B. M. Vickerman, E. M. Zywot, T. K. Tarrant and D. S. Lawrence, *Nat. Rev. Chem.*, 2021, **5**, 816–834.
5 G. C. Thaggard, J. Haimerl, K. C. Park, J. Lim, R. A. Fischer, B. K. P. M. Kankanamalage, B. J. Yarbrough, G. R. Wilson and N. B. Shustova, *J. Am. Chem. Soc.*, 2022, **144**, 23249–23263.
6 Z. Freixa, *Catal. Sci. Technol.*, 2020, **10**, 3122–3139.
7 M. Natali and S. Giordani, *Chem. Soc. Rev.*, 2012, **41**, 4010–4029.
8 F. A. Jerca, V. V. Jerca and R. Hoogenboom, *Nat. Rev. Chem.*, 2022, **6**, 51–69.
9 D. Villarón and S. J. Wezenberg, *Angew. Chem., Int. Ed.*, 2020, **59**, 13192–13202.
10 C. Petermayer and H. Dube, *Acc. Chem. Res.*, 2018, **51**, 1153–1163.
11 H.-B. Cheng, S. Zhang, E. Bai, X. Cao, J. Wang, J. Qi, J. Liu, J. Zhao, L. Zhang and J. Yoon, *Adv. Mater.*, 2022, **34**, 2108289.
12 L. Kortekaas and W. R. Browne, *Chem. Soc. Rev.*, 2019, **48**, 3406–3424.
13 S. Helmy, F. A. Leibfarth, S. Oh, J. E. Poelma, C. J. Hawker and J. Read de Alaniz, *J. Am. Chem. Soc.*, 2014, **136**, 8169–8172.
14 S. Helmy and J. Read de Alaniz, Photochromic and Thermochromic Heterocycles, *Advances in Heterocyclic Chemistry*, Elsevier Inc., 2015, vol. 117, pp 131–177.
15 M. M. Lerch, W. Szymanski and B. L. Feringa, *Chem. Soc. Rev.*, 2018, **47**, 1910–1937.
16 Y. Duan, H. Zhao, C. Xiong, L. Mao, D. Wang and Y. Zheng, *Chin. J. Chem.*, 2021, **39**, 985–998.
17 F. Stricker, S. Seshadri and J. Read de Alaniz, Donor-Acceptor Stenhouse Adducts, *Molecular Photoswitches: Chemistry, Properties, And Applications*, Wiley-VCH Gmbh, 2022, vol. 1, pp 303–324.

18 C. A. Reyes, A. Karr, C. A. Ramsperger, A. T. G. K, H. Lee and E. Picazo, *J. Am. Chem. Soc.*, 2025, **147**, 10–26.
19 Y. Huang, Y. Du, L. Luan, Z. Chu and L. He, *J. Macromol. Sci., Part A: Pure Appl. Chem.*, 2021, **58**, 717–724.
20 M. Clerc, S. Sandlass, O. Rifaie-Graham, O. J. A. Peterson, N. Bruns, J. Read de Alaniz and L. F. Boesel, *Chem. Soc. Rev.*, 2023, **52**, 8245–8294.
21 A. C. Overholts, W. Granados and M. J. Robb, *Nat. Chem.*, 2023, **15**, 332–338.
22 O. Rifaie-Graham, J. Yeow, A. Najer, R. Wang, R. Sun, K. Zhou, T. N. Dell, C. Adrianus, C. Thanapongpibul, M. Chami, S. Mann, J. Read de Alaniz and M. M. Stevens, *Nat. Chem.*, 2023, **15**, 110–118.
23 S. Seshadri, L. F. Gockowski, J. Lee, M. Sroda, M. E. Helgeson, J. Read de Alaniz and M. T. Valentine, *Nat. Commun.*, 2020, **11**, 2599.
24 S. Dubuis, A. Dellai, C. Courdurie, J. Owona, A. Kalafatis, L. Vellutini, E. Genin, V. Rodriguez and F. Castet, *J. Am. Chem. Soc.*, 2023, **145**, 10861–10871.
25 H. M. D. Bandara and S. C. Burdette, *Chem. Soc. Rev.*, 2012, **41**, 1809–1825.
26 J. Wu, L. Kreimendahl and J. L. Greenfield, *J. Am. Chem. Soc.*, 2025, **147**, 17549–17554.
27 M. Irie, *Chem. Rev.*, 2000, **100**, 1685–1716.
28 C. Schuschke, C. Hohner, M. Jevric, A. Ugleholdt Petersen, Z. Wang, M. Schwarz, M. Kettner, F. Waidhas, L. Fromm, C. J. Sumby, A. Görling, O. Brummel, K. Moth-Poulsen and J. Libuda, *Nat. Commun.*, 2019, **10**, 2384.
29 M. M. Lerch, S. J. Wezenberg, W. Szymanski and B. L. Feringa, *J. Am. Chem. Soc.*, 2016, **138**, 6344–6347.
30 M. Di Donato, M. M. Lerch, A. Lapini, A. D. Laurent, A. Iagatti, L. Bussotti, S. P. Ihrig, M. Medved, D. Jacquimin, W. Szymanski, W. J. Buma, P. Foggi and B. L. Feringa, *J. Am. Chem. Soc.*, 2017, **139**, 15596–15599.
31 J. N. Bull, E. Carroscosa, N. Mallo, M. S. Scholz, G. Silva, J. E. Beves and E. J. Bieske, *J. Phys. Chem. Lett.*, 2018, **9**, 665–671.
32 M. M. Lerch, M. Medved, A. Lapini, A. D. Laurent, A. Iagatti, L. Bussotti, W. Szymański, W. J. Buma, P. Foggi, M. Di Donato and B. L. Feringa, *J. Phys. Chem. A*, 2018, **122**, 955–964.
33 D. M. Sanchez, U. Raucci, K. N. Ferreras and T. J. Martinez, *J. Phys. Chem. Lett.*, 2020, **11**, 7901–7907.
34 D. M. Sanchez, U. Raucci and T. J. Martinez, *J. Am. Chem. Soc.*, 2021, **143**, 20015–20021.
35 U. Raucci, D. M. Sanchez and T. J. Martinez, *J. Am. Chem. Soc.*, 2022, **144**, 19265–19271.
36 Y. Li, C. Zhu, F. Gu and F. Liu, *Phys. Chem. Chem. Phys.*, 2023, **25**, 7417–7422.
37 H. Zulfikri, M. A. J. Koenis, M. M. Lerch, M. Di Donati, W. Szymanski, C. Filippi, B. L. Feringa and W. Jan Buma, *J. Am. Chem. Soc.*, 2019, **141**, 7376–7384.
38 T. Pradhan, D. K. Chelike, D. Roy, T. Pramanik and S. Dolui, *ACS Polym. Au*, 2025, **5**, 62–79.
39 M. M. Lerch, M. J. Hansen, W. A. Velema, W. Szymanski and B. L. Feringa, *Nat. Commun.*, 2016, **7**, 12054.
40 S. O. Poelma, S. S. Oh, S. Helmy, A. S. Knight, G. L. Burnett, H. T. Soh, C. J. Hawker and J. Read de Alaniz, *Chem. Commun.*, 2016, **52**, 10525–10528.
41 S. Helmy, S. Oh, F. A. Leibfarth, C. J. Hawker and J. Read de Alaniz, *J. Org. Chem.*, 2014, **79**, 11316–11329.
42 J. R. Hemmer, S. O. Poelma, N. Treat, Z. A. Page, N. D. Dolinski, Y. J. Diaz, W. Tomlinson, K. D. Clark, J. P. Hooper, C. Hawker and J. Read de Alaniz, *J. Am. Chem. Soc.*, 2016, **138**, 13960–13966.
43 N. Mallo, P. T. Brown, H. Iranmanesh, T. S. C. Macdonald, M. J. Teusner, J. B. Harper, G. E. Ball and J. E. Beves, *Chem. Commun.*, 2016, **52**, 13576–13579.
44 J. R. Hemmer, Z. A. Page, K. D. Clark, F. Stricker, N. D. Dolinski, C. J. Hawker and J. Read de Alaniz, *J. Am. Chem. Soc.*, 2018, **140**, 10425–10429.
45 D. Martinez-Lopez, E. Santamaria-Aranda, M. Marazzi, C. Garcia-Iriepa and D. Sampedro, *Chem. Eur. J.*, 2021, **27**, 4420–4429.
46 J. A. Peterson, F. Stricker and J. Read de Alaniz, *Chem. Commun.*, 2022, **58**, 2303–2306.
47 J. A. Peterson, N. M. Neris and J. Read de Alaniz, *Chem. Sci.*, 2023, **14**, 13025–13030.
48 A. V. Kulinich and A. A. Ishchenko, *Chem. Rev.*, 2024, **124**, 12086–12144.
49 F. Stricker, D. M. Sanchez, U. Raucci, N. D. Dolinski, M. S. Zayas, J. Meisner, C. J. Hawker, T. J. Martinez and J. Read de Alaniz, *Nat. Chem.*, 2022, **14**, 942–948.
50 C. A. Reyes, H. Lee, C. Karanovic and E. Picazo, *Nat. Commun.*, 2024, **15**, 5533.
51 G. Noirbent, Y. Xu, A.-H. Bonardi, S. Duval, D. Gigmes, J. Lalevée and F. Dumur, *Molecules*, 2020, **25**, 2317.
52 F. Stricker, J. Peterson and J. Read de Alaniz, *Org. Synth.*, 2022, **99**, 79–91.
53 M. Clerc, F. Stricker, S. Ulrich, M. Sroda, N. Bruns, L. F. Boesel and J. Read de Alaniz, *Angew. Chem., Int. Ed.*, 2021, **60**, 10219–10227.
54 V. V. Rostovtsev, L. G. Green, V. V. Fokin and K. B. Sharpless, *Angew. Chem., Int. Ed.*, 2002, **41**, 2596–2599.
55 L. F. Muff, L. Helwig, A. Nandi, C. M. Bates, C. J. Hawker and J. Read de Alaniz, *Angew. Chem., Int. Ed.*, 2025, **36**, e202514632.
56 P. Politzer and J. S. Murray, *J. Phys. Org. Chem.*, 2023, **36**, e4406.
57 R. Berraud-Pache, E. Santamaría-Aranda, B. de Souza, G. Bistoni, F. Neese, D. Sampedro and R. Izsák, *Chem. Sci.*, 2021, **12**, 2916–2924.
58 C. Zhang and X. Zhu, *Acc. Chem. Res.*, 2017, **50**, 1342–1350.
59 M. M. Sroda, F. Stricker, J. A. Peterson, J. Bernal and J. Read de Alaniz, *Chem. Eur. J.*, 2020, **27**, 4183–4190.
60 C. Reichardt, *Chem. Rev.*, 1994, **94**, 2319–2358.
61 C. Hansch, A. Leo and R. W. Taft, *Chem. Rev.*, 1991, **91**, 165–195.
62 F. Stricker, J. Peterson, S. K. Sandlass, A. de Tagyos, M. Sroda, S. Seshadri, M. J. Gordon and J. Read de Alaniz, *Chem*, 2023, **9**, 1994–2005.